Optical trapping with π-phase cylindrical vector beams

2010 New J. Phys. 12 073012

(http://iopscience.iop.org/1367-2630/12/7/073012)

New Journal of Physics
The open-access journal for physics

Optical trapping with π-phase cylindrical vector beams

Brian J Roxworthy[1,2] **and Kimani C Toussaint Jr**[1,2,3,4]

[1] Laboratory for Photonics Research of Bio/nano Environments (PROBE)
[2] Department of Mechanical Science and Engineering, University of Illinois at Urbana-Champaign, Urbana, IL 61801, USA
[3] Affiliate in the Departments of Electrical and Computer Engineering and Bioengineering, University of Illinois at Urbana-Champaign, Urbana, IL 61801, USA
[4] Affiliate, Beckman Institute for Advanced Science and Technology, University of Illinois at Urbana-Champaign, Urbana, IL 61801, USA

New Journal of Physics **12** (2010) 073012 (10pp)
Received 25 March 2010
Published 12 July 2010
Online at http://www.njp.org/
doi:10.1088/1367-2630/12/7/073012

Abstract. The use of π-phase radially and azimuthally polarized vector beams in optical trapping is investigated. We find that by tuning the relative phase between the eigenmodes comprising the beams, the optical forces applied to a trapped particle are modified. In particular, axial trapping efficiency is enhanced with increasing z polarization and the lateral trapping efficiency of the vector beams is reduced compared to a Gaussian input beam. In addition, this is the first experimental demonstration of low-power optical trapping in an aqueous environment using vector beams, which may have important applications in biological systems.

Contents

1. Introduction

Since the first demonstration of a stable three-dimensional (3D) optical trap, there have been many significant advances in the underlying theory and experimental implementation of optical tweezers [1]–[3]. The optimization of the trapping mechanism has been of particular interest for practical applications. For instance, methods to increase trap stability or efficiency have incorporated the use of feedback control schemes and holographic methods [4, 5]. Other approaches to achieving this rely on the use of specialized donut beams, which are characterized by their on-axis intensity null [6]–[8]. A particularly interesting class of donut beams are those that exhibit spatially dependent polarization over their cross sections. These vector beams come in many forms, such as radially and azimuthally polarized beams, and have been the subject of much research due to their peculiar focusing properties [9]–[19]. In particular, a highly focused radially polarized beam exhibits a strong axial electric field component, which for high numerical aperture (NA) can dominate the total electric field in the focal plane [12]. This z-polarized field has been observed using fluorescent probes [13] and has been proposed as a mechanism for linear accelerators [14].

In the case of optical trapping, radially polarized vector beams have recently attracted attention [15]–[20]. Since optical trapping requires large numerical apertures, using a radially polarized input beam will produce the aforementioned axial electric field. This z-polarized field produces an axial Poynting vector with a distinct null on axis, and for this reason the radially polarized beam is predicted to give increased axial trapping performance [15]. This has been verified theoretically for particles in both Mie and Rayleigh regimes [15]–[17]. Experimentally, Michihata *et al* [20] recently found that a high-power (100 mW) radially polarized beam produced an axial and lateral trap stiffness that was 1.19 and 0.8× that of a Gaussian beam, respectively. This was carried out using an objective lens with moderate numerical aperture (NA = 0.8–0.95), and for an 8 μm diameter glass microbead in a non-aqueous environment.

In the present work, we examine the axial and lateral trapping efficiencies (Q_{axial} and Q_{lateral}, respectively) of low-power (3 mW), π-phase vector beams under high-NA (NA = 1.25, oil) focusing (the prefix 'π' represents the relative phase between the eigenmodes that comprise the vector beam) as well as standard radial and azimuthal vector beams. Our approach is directly applicable to the common trapping scenario that utilizes high-NA lenses in an aqueous trapping environment, which is of particular importance to biological (trapping) applications that require low (laser)-power and high (spatial)-resolution imaging. Using 1 μm polystyrene beads, we compare the optical trapping performance of the π-phase and standard vector beams against a customary Gaussian input beam.

2. Theory

Conceptually, optical trapping concerns the competition between the gradient and scattering forces. The former is proportional to the intensity gradient of the focused optical field, and acts to pull a high-index (relative to the surrounding medium) particle into the high-intensity region of the focal field [21]. In the Mie regime, where the particle size is much larger than the optical wavelength, the scattering force can be interpreted as resulting primarily from the reflection of the s-polarized incident field from the particle surface [22, 23]. While the p-polarized field does contribute somewhat, its average reflection coefficient is 50% lower than that of the s-polarized field for the angles covered by a 1.25 NA objective. In the opposite Rayleigh regime, the particle size is much smaller than the wavelength, and the scattering force is interpreted in a dipole picture, where it is proportional to the time-averaged Poynting vector [24]. Determination of the scattering force in the intermediate-size regime is more challenging and relies on rigorous EM calculations using T-matrix or finite-difference time domain (FDTD) methods [25]. In all cases, the polarization structure and spatial intensity distribution of the focused trapping beam are important parameters for determining the optical forces on trapped particles.

We can express a Hermite–Gaussian beam with polarization components along the $\hat{\boldsymbol{x}}$ and $\hat{\boldsymbol{y}}$ directions by $\mathbf{E}_i = H_{nm}\hat{\mathbf{x}} + H_{nm}\hat{\mathbf{y}}$ [26] with

$$H_{nm} = A_0\, H_n\left(\frac{x}{w_0}\right) H_m\left(\frac{y}{w_0}\right) \exp\left(-\frac{x^2+y^2}{{w_0}^2}\right), \tag{1}$$

where A_0 is the field amplitude, w_0 is the beam waist diameter and $H_i(u)$ is a Hermite polynomial with index i. In order to model the input vector beams, we need only consider the first two modes of H_i given by $H_0(u) = 1$ and $H_1(u) = 2u$. Following the method of Richards and Wolf [26, 27], we find the electric field at the focal plane of an aplanatic lens (microscope objective) via

$$\mathbf{E}\,(\rho, \varphi, z) = A_{\rho\varphi z} \int_0^{2\pi} \int_0^{\theta_m} \mathbf{E}_0\,(\theta, \phi) \exp[\mathrm{j}k\rho \sin\theta \cos(\phi - \varphi)] \sin\theta \,\mathrm{d}\theta \,\mathrm{d}\phi, \tag{2}$$

where $\mathbf{E}_0$ is the refracted field just beyond the lens, $A_{\rho\varphi z} = \mathrm{j}\,kf \exp(-\mathrm{j}\,kf)/(2\pi)$, k is the wavenumber and f is the lens focal length, ρ and $\phi(\varphi)$ are the polar coordinates at the surface of the lens (focal plane) and θ is the coordinate obtained from refraction of ρ at the lens surface, and $\theta_m = \sin^{-1}(\mathrm{NA}/n_2)$ with NA = 1.25 and n_2 = 1.518. The refracted field in (2) is obtained by converting (1) to the spherical coordinates (f, θ, ϕ), which gives

$$\begin{aligned}\mathbf{E}_0\,(\theta, \phi) = {} & A_0 \sqrt{\frac{n_1}{n_2}\cos\theta}\; H_n\left(\frac{f\sin\theta\cos\phi}{w_0}\right) H_m\left(\frac{f\sin\theta\sin\phi}{w_0}\right) \exp\left(-\frac{f^2\sin^2\theta}{{w_0}^2}\right)\hat{\boldsymbol{x}} \\ & + A_0 \sqrt{\frac{n_1}{n_2}\cos\theta}\; H_n\left(\frac{f\sin\theta\,\cos\phi}{w_0}\right) H_m\left(\frac{f\sin\theta\sin\phi}{w_0}\right) \exp\left(-\frac{f^2\sin^2\theta}{{w_0}^2}\right)\hat{\boldsymbol{y}}, \end{aligned} \tag{3}$$

where

$$\hat{\boldsymbol{x}} = \cos\phi\hat{\boldsymbol{\theta}} - \sin\phi\hat{\boldsymbol{\phi}} \quad \text{and} \quad \hat{\boldsymbol{y}} = \sin\phi\hat{\boldsymbol{\theta}} + \cos\phi\hat{\boldsymbol{\phi}}\,, \tag{4}$$

with the standard spherical coordinate unit vectors given by $\hat{\boldsymbol{\theta}}$ and $\hat{\boldsymbol{\phi}}$. The additional term $[(n_1/n_2)\cos\theta]^{1/2}$ ensures conservation of energy across the lens [26]. Inasmuch as (3) represents a general input beam after refraction, we can express the specific beams used in

this study by the following formulae:

$$\begin{aligned}
\mathbf{E}_{0,\text{Gauss}} &= H_{00}\hat{\boldsymbol{x}},\\
\mathbf{E}_{0,\text{radial}} &= H_{10}\hat{\boldsymbol{x}} + H_{01}\hat{\boldsymbol{y}},\\
\mathbf{E}_{0,\pi\text{-radial}} &= H_{10}\hat{\boldsymbol{x}} - H_{01}\hat{\boldsymbol{y}},\\
\mathbf{E}_{0,\pi\text{-azimuthal}} &= -H_{01}\hat{\boldsymbol{x}} - H_{10}\hat{\boldsymbol{y}},\\
\mathbf{E}_{0,\text{azimuthal}} &= -H_{01}\hat{\boldsymbol{x}} + H_{10}\hat{\boldsymbol{y}},
\end{aligned} \tag{5}$$

where $\hat{\boldsymbol{x}}$ and $\hat{\boldsymbol{y}}$ are defined as in (4). The integral in (2) can be simplified by making use of the following identities:

$$\begin{aligned}
\int_0^{2\pi} \sin n\phi \exp[\mathrm{j}x\cos(\phi-\varphi)]\,\mathrm{d}\phi &= 2\pi \mathrm{j}^n J_n(x)\sin n\varphi,\\
\int_0^{2\pi} \cos n\phi \exp[\mathrm{j}x\cos(\phi-\varphi)]\,\mathrm{d}\phi &= 2\pi \mathrm{j}^n J_n(x)\cos n\varphi,
\end{aligned} \tag{6}$$

where J_n is a Bessel function of order n. Using (3)–(6), we can express (2) as a single integral over θ, which upon evaluation produces the electric field in the focal plane for various input beams. The focal intensities corresponding to each polarization component are given by $I_i = E_i \cdot E_i^*$, where $i = x, y, z$ and '$*$' represents complex conjugation. We therefore find the z-component of the focal intensity for each input beam via

$$\begin{aligned}
I_{z,\text{Gauss}} &= \frac{{w_0}^2}{f^2} C_{\rho\varphi z}\cos^2\varphi\left[\int_0^{\theta_m} A(\theta)\sqrt{\cos\theta}\sin^2\theta J_1(k\rho\sin\theta)\,\mathrm{d}\theta\right]\left[\ldots\right]^*,\\
I_{z,\text{radial}} &= 4C_{\rho\varphi z}\left[\int_0^{\theta_m} A(\theta)\sqrt{\cos\theta}\sin^3\theta J_0(k\rho\sin\theta)\,\mathrm{d}\theta\right]\left[\ldots\right]^*,\\
I_{z,\pi\text{-radial}} &= C_{\rho\varphi z}\left[-\int_0^{\theta_m} A(\theta)\sqrt{\cos\theta}\sin^3\theta J_0(k\rho\sin\theta)\,\mathrm{d}\theta + (\cos 2\varphi - \sin 2\varphi)\right.\\
&\quad\left.\times\int_0^{\theta_m} A(\theta)\sqrt{\cos\theta}\sin^3\theta J_2(k\rho\sin\theta)\,\mathrm{d}\theta\right]\left[\ldots\right]^*,\\
I_{z,\pi\text{-azimuthal}} &= C_{\rho\varphi z}\left[\int_0^{\theta_m} A(\theta)\sqrt{\cos\theta}\sin^3\theta J_0(k\rho\sin\theta)\,\mathrm{d}\theta - (\cos 2\varphi + \sin 2\varphi)\right.\\
&\quad\left.\times\int_0^{\theta_m} A(\theta)\sqrt{\cos\theta}\sin^3\theta J_2(k\rho\sin\theta)\,\mathrm{d}\theta\right]\left[\ldots\right]^*,\\
I_{z,\text{azimuthal}} &= 0,
\end{aligned} \tag{7}$$

where $C_{\rho\varphi z} = k^2 f^4 A_0^2 n_1/(w_0^2 n_2)$ and $A(\theta) = \exp[-(f^2\sin^2\theta/w_0^2)]$, which represents the objective filling parameter. In this case, a w_0 corresponding to a 10% overfilling of the objective back aperture is used. Similar expressions are used to find the total focal plane intensity of each beam, defined by $I_{\text{tot}} = I_x + I_y + I_z$, but are omitted here for brevity.

Using this formalism, the z-polarized and total focal intensity distributions for the various input beams are calculated by numerical integration and are shown in figure 1. The focal intensity distributions for each input beam are normalized with respect to each other, and the scale bars give the percentage of the maximum intensity present in each beam (e.g. the π-radial

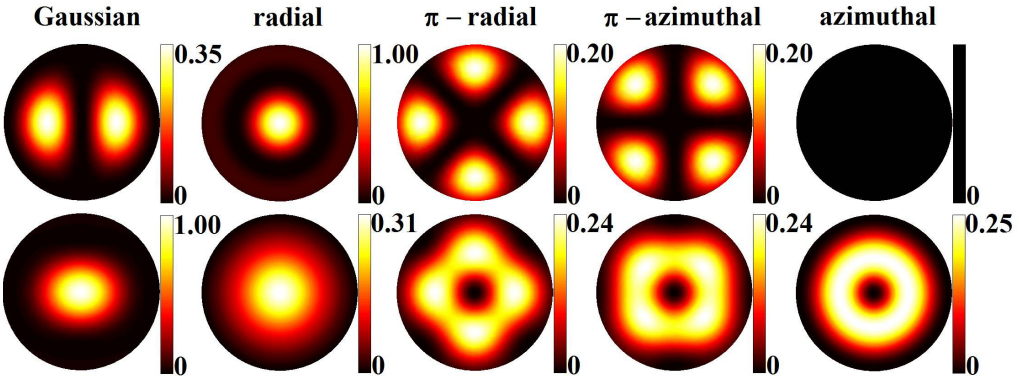

Figure 1. Simulated intensity distributions in the focal (x–y) plane for the input beams used for trapping. The top and bottom rows correspond to the axial and total intensity distributions, respectively. Each focal distribution is normalized to the maximum intensity in each row, and the scale bars indicate the fraction of the total intensity present in each intensity distribution.

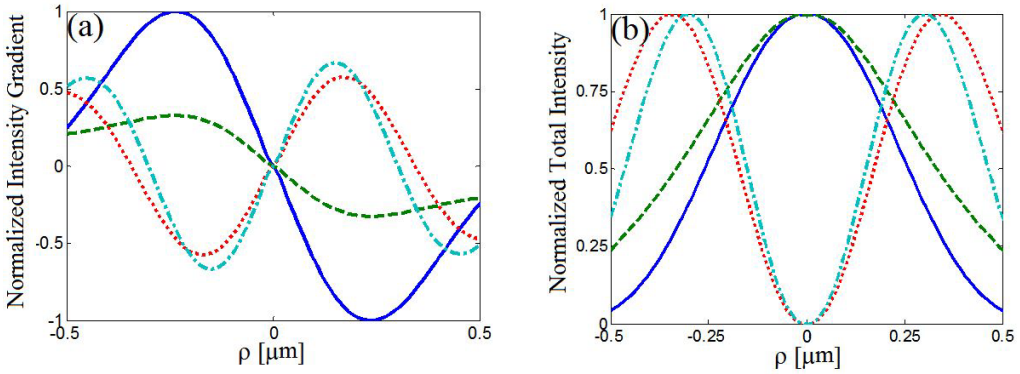

Figure 2. (a) Line plot of the normalized intensity gradient for the various input beams used in the experiment. (b) Line plot of the normalized total intensity distribution. In both plots, the beams are indicated by solid (blue)—Gaussian, dashed (green)—radial, dotted (red)—π-radial and dot-dashed (cyan)—azimuthal.

beam has 20% the value of z-polarized intensity present in the radial beam). It can be seen that the radial beam produces the largest z polarization, as expected.

The calculated focal intensity gradients for the beams are shown alongside their respective total intensity distributions in figure 2. Note that the π-azimuthal has the same profile as the π-radial, yet rotated by 45°; hence it is not included in the plots. Since the gradient force is proportional to the intensity gradient [21], figure 2(a) provides a visual comparison of the maximum gradient forces derived from each beam. From figure 2(b) we observe that the Gaussian and radial beams have comparable spot sizes (∼500 nm) whereas the spot sizes of the π-phase and azimuthal beams are considerably larger (∼900 and 800 nm, respectively). Note that the simulations are performed using the same conditions as stated for figure 1. It is clear that the intensity gradient is strictly negative (positive) for positive (negative) particle

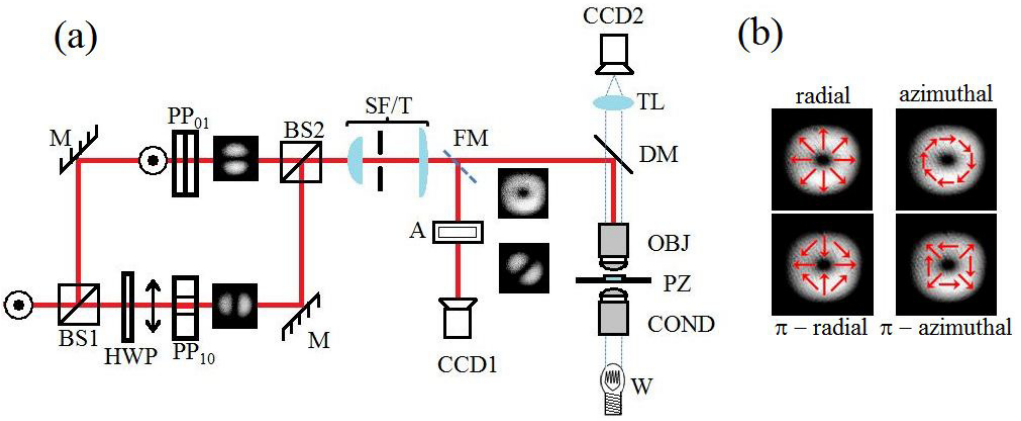

Figure 3. (a) Schematic of the experimental setup. A vertically polarized (with respect to the optical table, indicated by the out-of-plane arrow) input beam enters the Mach–Zehnder interferometer at the beamsplitter (BS1). In the lower arm, the beam encounters a half-wave plate (HWP) and is converted to horizontal polarization. In the π-radial configuration (shown), the phase plate (PP10) converts the beam to the HG10 mode and the upper phase plate (PP01) performs the complementary operation. The two modes are combined at BS2. Conversely, the π-azimuthal beams are created by switching PP10 and PP01. The spatial filter and telescope (SF/T) selects the fundamental donut mode and expands the beam to provide slight overfilling of the microscope objective (OBJ). A flip-mounted mirror (FM) is used to divert the beam through the analyzer (A) and image it onto a CCD camera (CCD1). The dichroic mirror (DM) couples the beam into the microscope, consisting of OBJ, a three-axis piezo-electric stage (PZ) and a condenser (COND). The white light source (W) provides illumination and the image is recorded at CCD2 via the tube lens (TL). The intensity patterns recorded at the various stages of the setup are included. (b) Experimental images of the vector beams with polarization distribution overlaid.

displacements for the radial and Gaussian input beams, which indicates that the gradient force always acts in the direction opposite to particle displacement, thereby serving to restore the particle to the trap center. Conversely, the sign changes in the intensity gradient for the π-phase and azimuthal beams imply that the gradient force (i) is only large over small regions in the focal plane, and (ii) does not always act opposite to the displacement, i.e. it sometimes acts to reject the particle.

3. Experiment

The experimental setup is shown in figure 3(a). A Mach–Zehnder interferometer equipped with tunable phase plates is used to create the vector beams, and the input beam derives from a 100 mW, 660 nm wavelength diode laser (Newport, LQC660-110C). The output of the interferometer is spatially filtered, expanded and coupled into a custom-built microscope, which consists of a 100× (1.25 NA) objective (Edmund Optics-NT43-905) and a 40× (0.65 NA) condenser (Newport-MV-40×). A white light source (Dolan Jenner, 190) is used to image the 1 μm

polystyrene particles (Duke Scientific) onto a CCD camera (Watec, 902H3-Ultimate). Using a flip mirror the output beam can be selectively diverted into the polarization analyzer arm, from which the purity of the vector beam polarization profile can be checked. In addition, the output can be switched to a Gaussian beam by blocking one arm of the interferometer and removing the phase plate from the remaining arm. For all beams, the power at the input to the microscope is kept constant at 3 mW. To tune the relative phase between the two eigenmodes to π, one simply extends the optical path length of a single phase plate. The various vector beams discussed previously are shown in figure 3(b).

The ability of an optical trap to convert incoming laser light (power) into a useful trapping force is measured using the dimensionless trapping efficiency parameter

$$Q = \frac{F_{\max} c}{n P}, \tag{8}$$

where $F_{\max}$ is the maximum trapping force exerted on the particle, c is the speed of light, n is the refractive index of the surrounding medium and P is the input laser power [22]. The trapping efficiency is assessed via the Stokes drag–force method in which we drive the sample stage at velocity v, inducing a drag force on the particle according to $F_{\text{drag}} = 6\pi\eta a\epsilon v$, where η is the dynamic viscosity of the medium, a is the radius of the particle and ϵ is Faxen's correction factor. We perform the experiments at a sufficient distance from the coverslip (8–10 μm) such that $\epsilon \approx 1$ and therefore does not affect (8) appreciably [23].

Following O'Neil and Padgett [28], a fully calibrated three-axis piezo-electric stage is used to vibrate the trapped particle with progressively increasing speed in the lateral and axial directions until it is ejected from the trap. These velocities are used to find the applied viscous drag force from which Q_{axial} and Q_{lateral} are calculated. This entire process is repeated 15 times for each input beam. To ensure accurate efficiency measurements, the power transmitted through the objective is measured using a sample cell filled with distilled water. We find that the power at the sample is 0.9 mW, giving 30% transmission of the 3 mW incident beam.

4. Results and discussion

Figure 4(a) shows the experimental trapping efficiency data taken over 15 runs, and the results are summarized in figure 4(b).

For the axial case, the radial beam has the largest trapping efficiency, which is 1.27× that of the Gaussian input beam. Moreover, we note that this result is consistent with what has been reported in the literature [20]. The two π-phase beams exhibit nearly the same trapping efficiency (∼0.120) and perform comparably with the Gaussian. Overall, the azimuthal beam is least efficient, giving a Q_{axial} 0.38× that of the radial. With the lateral case, the radial beam efficiency is 0.34× that of the Gaussian and is the largest for all vector beams. The π-phase beams again display congruous behavior, with efficiencies of about 0.25× that of the Gaussian. Lastly, the azimuthal beam performs quite poorly with respect to the other beams, showing a lateral trapping efficiency of 0.13× that of the Gaussian.

The axial performance of the various beams can be explained by examining the relative values of their z polarizations (figure 1, top row). The experimentally obtained axial trapping efficiencies follow exactly the order of simulated axial intensity magnitude in each beam. Most notably, the radial beam, which has the largest z polarization, produces a Q_{axial} that is 2.6× that of the azimuthal beam, which exhibits an identically zero z polarization. The two π-phase beams

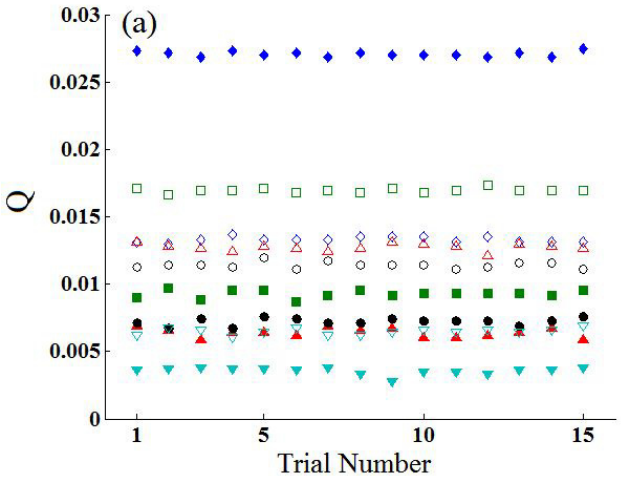

(b)

Trapping Efficiency	Q_{axial}	$Q_{lateral}$
G	0.0133	0.0271
RP	0.017	0.0093
π - RP	0.0127	0.0064
π - AP	0.0114	0.0072
AP	0.0065	0.0036

Figure 4. (a) Experimentally obtained trapping efficiency values. Solid markers indicate lateral trapping efficiency whereas open markers indicate axial trapping efficiency. The input beams are indicated by diamond—Gaussian, square—radial, circle—π-radial, upward triangle—π-azimuthal and downward triangle—azimuthal. (b) Experimental trapping efficiency values for the various beams.

produce identical amounts of z polarization, at 0.20× that of the radial, and correspondingly yield similar axial trapping efficiencies. Furthermore, these two beams give slightly reduced performance compared to the Gaussian, which produces a larger axial intensity, at 0.35× that of the radial.

The role of spot size on the axial performance of the various beams appears relatively small compared to the role of z polarization. From figure 2(b) it can be seen that the π-radial (π-azimuthal) and Gaussian beams have spot sizes of ∼900 and 450 nm, respectively. However, the π-phase beams perform comparably to the Gaussian in the axial direction. This fact suggests that z polarization is the dominant factor in providing a large Q_{axial}. This is further evidenced by examining the radial beam, which produces 2.8× the z polarization and 1.27× the Q_{axial} for the Gaussian beam, while having a comparable focal spot size.

Trapping among vector beams in the lateral direction is consistent with what is expected given the focal spot size. Namely, the radial beam has a smaller spot size than all the other vector beams and yields a 1.45×, 1.29× and 2.6× increase in Q_{lateral} compared to the π-radial, π-azimuthal and azimuthal beams, respectively. Further, while all vector beams have similar maximum intensity gradient values, the modulation of the intensity gradient in the focal plane for the π-radial, π-azimuthal and azimuthal beams likely leads to their lower Q_{lateral} values in comparison with the radial beam. The largest Q_{lateral} is observed for the Gaussian input beam (0.027), which is expected since it produces the largest intensity gradient.

5. Conclusion

Our results confirm that the axial trapping efficiency can be optimized by the amount of z polarization produced in the focal plane. Further, we find that even in a low-power trapping environment, a radial vector beam is advantageous over a Gaussian beam for axial trapping,

and the π-phase vector beams produce axial trapping efficiencies comparable to that of the Gaussian. Additionally, this study demonstrates that the relative phase between the eigenmodes comprising the vector beams is an important parameter for tuning the trapping force applied by the vector beams. Currently, we are investigating the trapping efficiency for vector beams with relative phases other than π, which may result in an input beam that optimizes both Q_{lateral} and Q_{axial}.

Acknowledgments

This work was supported by the University of Illinois at Urbana-Champaign research startup funds. We thank Santosh Tripathi for help with the focal field simulations. We also thank the reviewers for encouraging remarks and suggestions which improved the overall quality of the paper.

References

[1] Ashkin A, Dziedzic J M, Bjorkholm J E and Chu S 1986 Observation of a single-beam gradient force optical trap for dielectric particles *Opt. Lett.* **11** 288–90
[2] Gittes F and Schmidt C F 1998 Interference model for back-focal-plane displacement detection in optical tweezers *Opt. Lett.* **23** 7–9
[3] Prentice P A, MacDonald M P, Frank T G, Cuschieri A, Spalding G C, Sibbett W, Cambell P A and Dholakia K 2004 Manipulation and filtration of low index particles with holographic Laguerre-Gaussian optical trap arrays *Opt. Express* **12** 593–600
[4] Sun B, Roichman Y and Grier D G 2008 Theory of holographic optical trapping *Opt. Express* **16** 15765–76
[5] Lang M J, Asbury C L, Shaevitz J W and Block S M 2002 An automated two-dimensional optical force clamp for single molecule studies *Biophys. J.* **83** 491–501
[6] Simpson N B, McGloin D, Dholakia K, Allen L and Padgett M J 1998 Optical tweezers with increased axial trapping efficiency *J. Mod. Opt.* **45** 1943–9
[7] Gao C, Gao M and Weber H 2004 Generation and application of twisted hollow beams *Optik* **115** 129–33
[8] Allen L, Beijersbergen M W, Spreeuw R J C and Woerdman J P 1992 Orbital angular momentum of light and the transformation of Laguerre–Gaussian laser modes *Phys. Rev.* A **45** 8185–9
[9] Maurer C, Jesacher A, Fürhapter S, Bernet S and Ritsch-Marte M 2007 Tailoring of arbitrary optical vector beams *New J. Phys.* **9** 78
[10] Zhan Q 2009 Cylindrical vector beams: from mathematical concepts to applications *Adv. Opt. Photon.* **1** 1–57
[11] Wang X L, Ding J, Ni W J, Guo C S and Wang H T 2007 Generation of arbitrary vector beams with a spatial light modulator and a common path interferometric arrangement *Opt. Lett.* **32** 3549–51
[12] Youngworth K S and Brown T G 2000 Focusing of high numerical aperture cylindrical-vector beams *Opt. Express* **7** 77–87
[13] Novotny L, Beversluis M R, Youngworth K S and Brown T G 2001 Longitudinal field modes probed by single molecules *Phys. Rev. Lett.* **86** 5251–4
[14] Serafim S, Sprangle P and Hafizi B 2000 Optical guiding of a radially polarized laser beam for inverse Cherenkov acceleration in a plasma channel *IEEE Trans. Plasma Sci.* **28** 1155–8
[15] Zhan Q W 2003 Radiation forces on a dielectric sphere produced by highly focused cylindrical vector beams *J. Opt. A: Pure Appl. Opt.* **5** 229–32
[16] Kawauchi H, Yonezawa K, Kozawa Y and Sato S 2007 Calculation of optical trapping forces on a dielectric sphere in the ray optics regime produced by a radially polarized laser beam *Opt. Lett.* **32** 1839–41
[17] Nieminen T A, Heckenberg N R and Rubinsztein-Dunlop H 2008 Forces in optical tweezers with radially and azimuthally polarized trapping beams *Opt. Lett.* **33** 122–4

[18] Peng F, Yao B L, Yan S H, Zhao W and Lei M 2009 Trapping of low-refractive-index particles with azimuthally polarized beam *J. Opt. Soc. Am. B: Opt. Phys.* **26** 2242–7
[19] Yan S H and Yao B L 2007 Radiation forces of a highly focused radially polarized beam on spherical particles *Phys. Rev.* A **76** 6
[20] Michihata M, Hayashi T and Takaya Y 2009 Measurement of axial and transverse trapping stiffness of optical tweezers in air using a radially polarized beam *Appl. Opt.* **48** 6143–51
[21] Rohrbach A 2005 Stiffness of optical traps: quantitative agreement between experiment and electromagnetic theory *Phys. Rev. Lett.* **95** 168102
[22] Ashkin A 1992 Forces of a single-beam gradient laser trap on a dielectric sphere in the ray optics regime *Biophys. J.* **61** 569–82
[23] Neuman K C and Block S M 2004 Optical trapping *Rev. Sci. Instrum.* **75** 2787–809
[24] Toussaint K C Jr, Liu M, Pelton M, Pesic J, Guffey M J, Guyot-Sionnest P and Scherer N F 2007 Plasmon resonance-based optical trapping of single and multiple Au nanoparticles *Opt. Express* **15** 12017–29
[25] Qin J Q, Wang X L, Jia D, Chen J, Fan Y X, Ding J P and Wang H T 2009 FDTD approach to optical forces of tightly focused vector beams on metal particles *Opt. Express* **17** 8407–16
[26] Novotny L and Hecht B 2006 *Principles of Nano-Optics* (Cambridge: Cambridge University Press)
[27] Richards B and Wolf E 1959 Electromagnetic diffraction in optical systems II. Structure of the image field in an aplanatic system *Proc. R. Soc.* A **253** 358–79
[28] O'Neill A T and Padgett M J 2001 Axial and lateral trapping efficiency of Laguerre–Gaussian modes in inverted optical tweezers *Opt. Commum.* **193** 45–50